Journal of Marine Research, 63, 813–839, 2005

Preformed phosphate, soft tissue pump and atmospheric CO_2

by Takamitsu Ito[1,2] and Michael J. Follows[1]

ABSTRACT

We develop a new theory relating atmospheric pCO_2 and the efficiency of the soft tissue pump of CO_2 in the ocean, measured by P^*, a quasi-conservative tracer. P^* is inversely correlated with preformed phosphate, and its global average represents the fraction of nutrients transported by the export and remineralization of organic material. This view is combined with global conservation constraints for carbon and nutrients leading to a theoretical prediction for the sensitivity of atmospheric pCO_2 to changes in globally averaged P^*. The theory is supported by sensitivity studies with a more complex, three-dimensional numerical simulations. The numerical experiments suggest that the ocean carbon cycle is unlikely to approach the theoretical limit where globally averaged $P^* = 1$ (complete depletion of preformed phosphate) because the localized dynamics of deep water formation, which may be associated with rapid vertical mixing timescales, preclude the ventilation of strongly nutrient-depleted waters. Hence, in the large volume of the deep waters of the ocean, it is difficult to significantly reduce preformed nutrient (or increase P^*) by increasing the efficiency of export production. This mechanism could ultimately control the efficiency of biological pumps in a climate with increased aeolian iron sources to the Southern Ocean. Using these concepts we can reconcile qualitative differences in the response of atmospheric pCO_2 to surface nutrient draw down in highly idealized box models and more complex, general circulation models. We suggest that studies of carbon cycle dynamics in regions of deep water formation are the key to understanding the sensitivity of atmospheric pCO_2 to biological pumps in the ocean.

1. Introduction

Photosynthesis in the surface ocean converts inorganic carbon and nutrients into organic matter, often accompanied by calcium carbonate structural material. The living tissues take part in complex ecosystem behavior and local remineralization, but a fraction, described as export production, is ultimately transported to, and remineralized within, thermocline and abyssal ocean. The vertical transport of organic carbon is termed the soft tissue pump and that of calcite, the carbonate pump (Volk and Hoffert, 1985). These biological carbon pumps remove carbon from surface oceans and the atmosphere and store it in the ocean interior, and might play a critical role in the long-term variation of atmospheric CO_2.

1. Department of Earth, Atmospheric and Planetary Sciences, Massachusetts Institute of Technology, Cambridge, Massachusetts, 02139, U.S.A.

2. Present address: Joint Institute for the Study of the Atmosphere and the Ocean, University of Washington, Box 354235, Seattle, Washington, 98195-4235, U.S.A. ***email: ito@atmos.washington.edu***

Polar ice cores suggest that atmospheric pCO_2 significantly fluctuated between 180 ppm during the cold, glacial periods and 280 ppm during the warm, interglacial periods (Petit *et al.,* 1999). Box model studies (Sarmiento and Toggweiler, 1984; Siegenthaler and Wenk, 1984; Knox and McElroy, 1984) illustrated that atmospheric CO_2 is highly sensitive to the depletion of high latitude surface nutrients. Following these studies, several possible mechanisms have been suggested for the depletion of high latitude surface nutrients, for example, reduced ocean ventilation (Francois *et al.,* 1997) and increased export production (Kumar *et al.,* 1995) which may be related to changes in iron limitation of phytoplankton organisms in the Southern Ocean (Martin, 1990). However, a recent study based on more complicated, and perhaps more realistic, general circulation models showed that depletion of surface nutrient leads to a weaker response in atmospheric CO_2 and cannot fully reproduce glacial-interglacial changes in atmospheric pCO_2 (Archer *et al.,* 2000). How can we define and quantify the efficiency of biological pumps independent of the types of numerical models? What ultimately controls the efficiency of the biological pumps in the oceans? Can we reconcile the box model and GCM results? First we briefly review the measures by which the efficiency of the biological carbon pumps have been defined.

a. Vertical gradients of DIC and nutrients

Volk and Hoffert (1985) first defined the biological (and solubility) pumps of carbon, characterizing their relative efficiency in terms of their contributions to the vertical gradient of DIC. For a closed ocean-atmosphere system, increasing the vertical gradient in DIC reduces the DIC concentration in the surface oceans. Since the surface oceans, on global average, are indeed close to equilibrium with atmospheric CO_2, this reduces atmospheric pCO_2. In addition to the biological pumps, vertical gradient of DIC is enhanced by the thermal structure of the ocean and its control on the solubility of CO_2 (solubility pump of CO_2). Cold and dense deep waters are enriched in DIC relative to the warm surface waters. Preindustrial atmosphere contained 280 ppmv of CO_2 as a result of the combined effects of the solubility pump and the biological pumps. For example, box models suggest that atmospheric pCO_2 would rise to approximately 460 ppmv (Sarmiento and Toggweiler, 1984; Volk and Hoffert, 1985) if the effects of the biological pumps were completely removed. When the effects of both solubility pump and biological pumps were removed by homogenizing the DIC concentration in the oceans, atmospheric pCO_2 would rise up to 720 ppmv (Volk and Hoffert, 1985). The vertical gradient of DIC is an useful measure for interpreting idealized conceptual models. However, this one-dimensional view cannot address the role of the significant horizontal variabilities observed in the real ocean.

b. Unutilized surface macro-nutrients

The efficiency of the biological carbon pumps has also been related to the budget of macro-nutrients (nitrate or phosphate) in the surface ocean. The presence of inorganic nutrients in the surface waters suggests that the soft tissue pump of carbon is not working at

full efficiency. There are large regions of the surface ocean, in particular the high latitude Southern Oceans, where surface macro-nutrients are far from depleted. If the available nutrients were to be consumed in photosynthesis and transferred to the deep ocean as organic matter, they might significantly enhance the storage of carbon in the deep ocean. Classical box model studies indicated that completely depleting the surface nutrients in the Southern Ocean can drive down atmospheric pCO_2 as low as 165 ppmv (Sarmiento and Toggweiler, 1984), approximately 115 ppmv lower than preindustrial condition. They predict that atmospheric CO_2 can change on the order of 300 ppmv between the case with complete utilization of surface nutrients and the case with no biological export and remineralization. Recent studies, in contrast, suggest that drawing down surface nutrients in general circulation and biogeochemistry models has a weaker response in atmospheric CO_2. GCM simulations with a rapid Newtonian damping of surface nutrients result in a decrease of 46–84 ppmv (Sarmiento and Orr, 1991) and approximately 50 ppmv (Archer *et al.,* 2000). These results indicate that the simulated sensitivity of atmospheric CO_2 in GCMs is significantly smaller than that of box models. Inventories of macro-nutrient in the surface ocean are unlikely to be a robust measure of the efficiency of biological pump since the sensitivity depends on the model architecture. Here we develop a new measure of the efficiency of the biological pump, which is independent of the formulation and the spatial resolution of the model.

In Section 2 we develop a simple mathematical model describing the efficiency of the soft tissue pump in terms of the fraction of nutrients which are "preformed," and predict the sensitivity of atmospheric pCO_2 to the inventory of preformed nutrients. A key element of the theory is the integral constraint on the carbon and nutrient budgets, and partitioning of carbon and nutrients between the "preformed" pool and the "regenerated" pool. In Section 3 we use an ocean GCM and biogeochemistry model to simulate ocean carbon pumps and partitioning of CO_2 between atmosphere and ocean. We use the numerical model to evaluate theoretical predictions against sensitivity experiments. Furthermore, the sensitivity experiments can illustrate bounds on the potential range of variation in atmospheric CO_2, and we discuss constraints on the role of the biological pumps in controlling atmospheric CO_2 over glacial-interglacial timescales.

2. Theory and observations

First we review concepts of preformed and regenerated nutrients and illustrate them using observed tracer distributions from WOCE-JGOFS survey and climatology (Conkright *et al*., 2002). It is possible to define two components in nutrient and carbon concentrations: the "preformed" component and the "regenerated" component. The partitioning between the two pools plays critical roles in setting the efficiency of the soft tissue pump and its control on atmospheric CO_2. Then we develop a simple mathematical model describing the efficiency of the soft tissue pump combining the partitioning of nutrient and carbon with global conservation constraints. The theory, in turn, gives insights into the interpretation of the observations and the quantification of the soft tissue pump.

a. Preformed and regenerated phosphate

We consider phosphate as a measure of macro-nutrient, and write it as the sum of preformed phosphate and regenerated phosphate.

$$P = P_{pre} + P_{reg}. \tag{1}$$

When thermocline or deep waters are newly formed, unutilized nutrients are subducted into the interior ocean. The fraction of nutrient in the ocean which was subducted and transported is termed "preformed" nutrient, P_{pre} (Broecker, 1974; Broecker and Peng, 1982; Broecker *et al.,* 1985; Toggweiler *et al.,* 2003b; Sigman and Haug, 2003). In the interior ocean, phosphate is added to the waters through respiration of organic molecules. Clearly the preformed phosphate of the deep waters is closely related to the surface concentration at the outcrop of isopycnals (Broecker *et al.,* 1985). The fraction of phosphate in the ocean which is regenerated by respiration is termed "regenerated" nutrient, P_{reg}.

Regenerated phosphate, P_{reg}, can be estimated using Apparent Oxygen Utilization (AOU), which depends on the observed temperature, salinity and *in-situ* oxygen distributions (Broecker, 1974; Broecker *et al.,* 1985). In the interior ocean, O_2 is consumed by respiration, and generally, oxygen is increasingly depleted as the water mass accumulates regenerated nutrients. Assuming that oxygen concentration is close to saturation at the surface, we can estimate how much oxygen is consumed by the remineralization of organic molecules.

$$AOU = O_{2,sat}(T, S) - O_2 \tag{2}$$

$$P_{reg} = R_{P:O2}AOU \tag{3}$$

where $O_{2,sat}$ is the saturated concentration of oxygen which is a function of temperature, T and salinity, S. We assume a fixed stoichiometric ratio between oxygen, phosphate and organic carbon following Anderson (1995). Figure 1 shows the distribution of regenerated phosphate in the Atlantic and Pacific ocean from WOCE lines A-17 and A-20 for Atlantic, and P-18 for Pacific. Regenerated phosphate generally increases with the "age" of the water due to the accumulation of biogenic phosphate. Newly ventilated NADW contains less regenerated phosphate, P_{reg}, and it has a maximum value in the deep North Pacific.

Figure 2 shows the distribution of preformed phosphate in the Atlantic and Pacific section, revealing the contrast between major water masses in the global ocean: the waters formed in the northern North Atlantic (NADW) are relatively low (~0.9 μM) in preformed nutrient. The waters formed in the Southern Ocean are relatively enriched (~1.6 μM), reflecting high surface nutrient concentration of the region of water mass formation. Mode waters in subtropical thermocline are depleted in preformed phosphate (0.6 μM); much lower than the deep waters since they are formed at middle latitudes. In the Antarctic Circumpolar Current, (ACC) deep waters from the northern North Atlantic are mixed with the waters formed in the Southern Ocean.

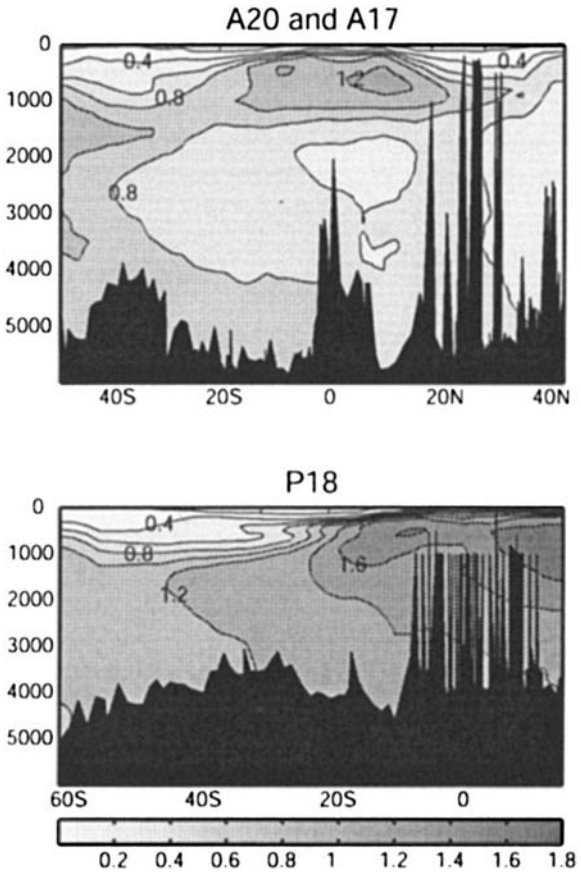

Figure 1. Distribution of P_{reg}, regenerated phosphate based on the WOCE-JGOFS survey. (a) WOCE line A-17 and A-20 in the Atlantic Ocean, (b) WOCE line P-18 in the Pacific Ocean. We use *in-situ* oxygen and hydrographic data to calculate AOU. Observed data is interpolated on to a latitude-depth grid whose horizontal resolution is 1° and vertical resolution is 100 m. While general patterns of AOU clearly indicate the integrated effect of respiration, one has to be cautious about its interpretation. Significant undersaturation of oxygen and other trace gases is observed in the ice-covered surface polar oceans (Weiss *et al.,* 1979; Schlosser *et al.,* 1991), suggesting that preformed oxygen concentration may be lower than saturation particularly in the cold deep waters. If preformed oxygen concentration is undersaturated, AOU overestimates the effect of respiration and so does the regenerated phosphate (Ito *et al.,* 2004).

Figure 3 schematically illustrates the nutrient cycle in the oceans, and offers a qualitative interpretation of the partitioning of phosphate between the "preformed" pool and the "regenerated" pool. Nutrients are supplied to the surface oceans by physical transport such as upwelling of intermediate and deep waters. There are two pathways for nutrients to return back into the interior ocean: (1) through biological export and remineralization (biological path), and (2) through subduction and water mass formation (physical path).

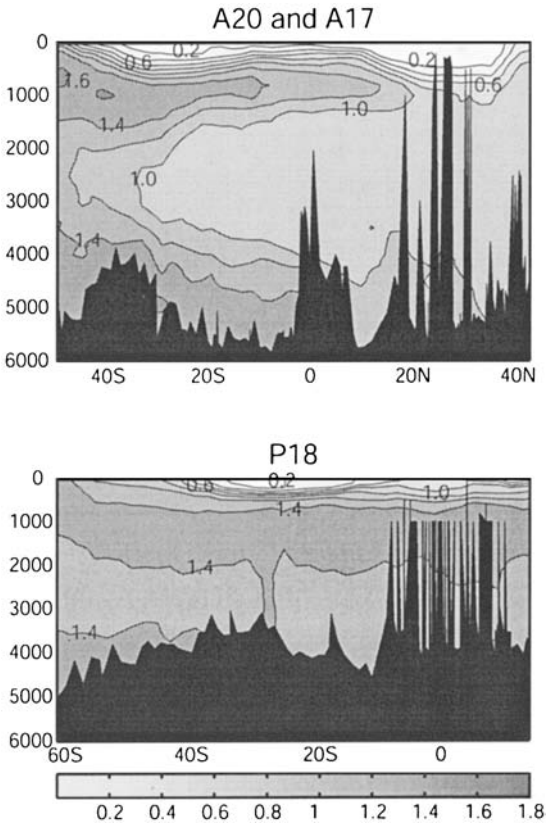

Figure 2. Preformed phosphate distribution based on WOCE-JGOFS survey. Data are taken from (a) line A-17 and A-20, (b) line P-18. Waters formed in the Southern Ocean have approximately 1.6 μM of preformed phosphate based on the calculation using AOU (2) which may include a bias due to the oxygen disequilibrium. (See caption for Fig. 1.)

The contrast between the two pathways can clearly illustrate the efficiency of the soft tissue pump. The biological path is associated with sequestration of carbons from the surface oceans, which is efficient in driving down atmospheric CO_2. In contrast the biological pumps do not operate through the physical path.

The relative significance of the two pathways can be illustrated using the concept of preformed and regenerated nutrient. The distribution of the regenerated phosphate (shown in Fig. 1) reflects the integrated effect of phosphate returning to the interior ocean through the "biological" path. Similarly the pattern of the preformed phosphate (shown in Fig. 2) reveals the amount of phosphate returning to the interior ocean through the "physical" path.

Let us consider an extreme case in which surface phosphate is totally depleted by biological uptake. All the upwelling phosphate return to the interior ocean through the "biological path." In this limit case the soft tissue pump is working at its maximum

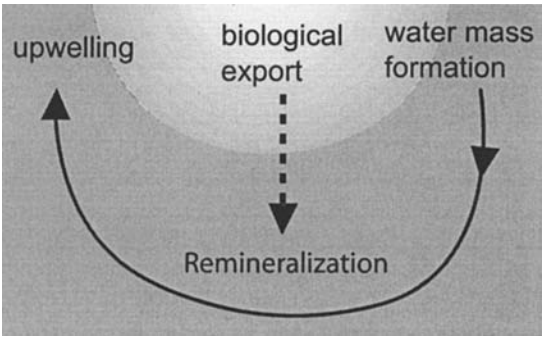

Figure 3. A schematic diagram for the major pathways of macro-nutrients in the oceans. The upwelling of nutrient is balanced by (1) biological uptake and export and by (2) subduction and formation of water masses. Here we neglect the effects of riverine input and sedimentary burial.

efficiency ($P_{pre} = 0$). Another limit case is that there is no biological uptake at all. All the upwelling nutrients return to the interior ocean through the "physical path." This corresponds to the minimum efficiency of the soft tissue pump ($P_{reg} = 0$). There is no regenerated nutrients in the oceans, and all the nutrients are preformed. Biological pump of the real ocean should fall somewhere in between the two limit cases.

Here we define a global metric of the efficiency of the soft tissue pump, $\overline{P^*}$, reflecting the fraction of phosphate which is regenerated by respiration in the global ocean. It quantitatively indicates the importance of the biological path in the downwards return of nutrients to the interior ocean.

$$\overline{P^*} \equiv \frac{\overline{P_{reg}}}{\bar{P}} \tag{4}$$

where $\bar{P}$ is the global mean of P. $\overline{P^*}$ can only vary between 0 and 1: $\overline{P^*} = 1$ indicates the complete utilization of phosphate in the surface oceans, and $\overline{P^*} = 0$ indicates a complete shutdown of the soft tissue pump. We use $\overline{P^*}$ as a global measure of the efficiency of the soft tissue pump, which can be calculated from the distributions of phosphate and oxygen in observations and models.

The efficiency of the soft tissue pump of the modern ocean can be readily calculated based on climatological distributions of phosphate and oxygen, using the World Ocean Atlas (Conkright *et al.,* 2002). Applying Eq. (2, 3, 4) to the climatological distribution of T, S, P and O_2, we find that $\overline{P^*}$ is approximately 0.36 indicating that about 36% of phosphate is in the regenerated pool in the modern ocean. What is the expected range of atmospheric CO_2 associated with the variation in $\overline{P^*}$? In the following sections we develop a mathematical model describing the relationship between $\overline{P^*}$ and atmospheric pCO_2.

b. Carbon pump decomposition

First we describe the decomposition of the DIC concentration into carbon pumps components. Carbon pump decomposition was first introduced as a tool for detecting

anthropogenic CO_2 in the ocean (Brewer, 1978; Chen and Millero, 1979). The approach has been modified and developed into the ΔC^* method used for the same purpose (Gruber *et al.,* 1996; Gruber, 1998; Sabine *et al.,* 1999). In a variation of this approach, Gruber and Sarmiento (2002) also analyzed the carbon pump components of observed tracer fields from the recent WOCE-JGOFS survey and illustrated the processes controlling the vertical gradient of DIC, in which tracer fields are referenced to the global surface mean properties. Here we decompose the carbon pumps based on the partitioning of DIC between the preformed pool and the regenerated pool where tracer fields are referenced to the outcrop of isopycnals.

As for the partitioning of phosphate (1), observed DIC concentration, C, can be expressed as the sum of preformed DIC, C_{pre}, and regenerated DIC, C_{reg}.

$$C = C_{pre} + C_{reg}. \tag{5}$$

C_{reg} can be further divided into a soft tissue component and a calcite component representing the respiration of organic molecules and the dissolution of calcium carbonate structural materials.

$$C_{reg} = C_{calcite} + C_{org} \tag{6}$$

$$C_{org} = R_{Corg:PO_4} P_{reg}. \tag{7}$$

Regenerated phosphate, P_{reg}, and the soft tissue component, C_{org}, are coupled assuming a constant stoichiometric ratio (Anderson, 1995). Preformed carbon concentration, C_{pre}, can be decomposed into the saturated component (i.e. the concentration at equilibrium with preindustrial atmosphere) and ΔC^*.

$$C_{pre} = C_{sat}(T, S, TA_{pref}, pCO_2^{atm}) + \Delta C^*. \tag{8}$$

ΔC^* therefore contains components due to both anthropogenic CO_2 and air-sea disequilibrium under preindustrial conditions. Here we consider only the preindustrial condition where there is no influence of anthropogenic CO_2, and we use the notation, ΔC, for preindustrial disequilibrium. For example, if surface waters at an outcrop are in complete saturation with overlying atmospheric pCO_2, $\Delta C = 0$. A positive ΔC indicates that the surface waters were outgassing CO_2 into the atmosphere at the time of subduction. Similarly, a negative ΔC indicates uptake. In the following section we combine the carbon pump decomposition, the partitioning of phosphate and the integral constraints for carbon and nutrients to form a new theory for calculating the sensitivity of atmospheric CO_2.

c. A new theory based on the integral constraints on carbon and phosphate

Here we explore the connection between the soft tissue pump, expressed in terms of $\overline{P^*}$, and atmospheric CO_2, and derive a general theory for constraining the efficiency of soft tissue pump. We illustrate the coupling between the preformed phosphate and atmospheric pCO_2 based on the integrated mass balance of carbon and nutrients in the ocean-

atmosphere system. The mass balance constraints are independent of the detailed physical and biogeochemical parameterization, and are generally applicable to models with wide range of complexity. First, we assume that the ocean-atmosphere system is in closed balance so that we may neglect riverine input and sedimentary interactions of nutrients and carbon. Here we also neglect the changes in carbon and nutrients stored in the land biosphere and soil in order to focus on the effect of changes in the oceanic processes. The timescale for mixing of CO_2 in the atmosphere is rapid relative to relevant oceanic processes, and the atmosphere can be treated as a well-mixed reservoir of CO_2. The global conservation of phosphate and carbon can be stated as following:

$$P_0 = \frac{1}{V}\int_V P\, dxdydz = constant. \tag{9}$$

$$C_0 = \frac{1}{V}\left(MpCO_2^{atm} + \int_V C\, dx\, dy\, dz\right) = constant. \tag{10}$$

M is the total moles of gas in the atmosphere, pCO_2^{atm} is the mixing ratio of atmospheric CO_2. V represents the volume of the global ocean. P and C are the ocean phosphate and dissolved inorganic carbon concentration in units of mol m^{-3}. We assume the conservation of the total amount of phosphate and carbon in the atmosphere-ocean system.

The integral constraint (10) and carbon pump components (5, 6, 8) can be combined to yield an expression for the partitioning of carbon between the atmospheric reservoir and the carbon pumps in the ocean.

$$MpCO_2^{atm} + V\{\overline{C_{sat}} + \overline{\Delta C} + \overline{C_{org}} + \overline{C_{calcite}}\} = VC_0 \tag{11}$$

where VC_0 represents the total amount of carbon in the system, and the overbar indicates globally averaged concentrations. M, V and C_0 are assumed to be constants of the system. It is interesting to consider the sensitivity of atmospheric CO_2 by making a small perturbation to a reasonable mean state. For small perturbations to the carbon pump components, Eq. (11) becomes

$$M\delta pCO_2^{atm} + V\{\delta\overline{C_{sat}} + \delta\overline{\Delta C} + \delta\overline{C_{org}} + \delta\overline{C_{calcite}}\} = 0. \tag{12}$$

Here we will specifically consider the sensitivity of pCO_2^{atm} to the soft tissue pump. For simplicity we assume that a perturbation in the soft tissue pump is decoupled from that of the carbonate pump and the degree of saturation, so, we set $\delta\overline{C_{calcite}} = \delta\overline{\Delta C} = 0$. The relationship between C_{sat} and pCO_2^{atm} are determined by the carbonate chemistry of the sea water. For a simple case where T, S and Alk are held constant, variations in C_{sat} and pCO_2^{atm} can be described using the Buffer factor, $B \sim 10$ (Bolin and Eriksson, 1959).

$$\delta \ln pCO_2^{atm} = B\delta \ln C_{sat} \tag{13}$$

There are spatial variations in C_{sat} in the surface ocean but the variation of C_{sat} is one order of magnitude smaller than its mean value. Thus it can be shown that $\overline{\ln C_{sat}} = \ln \overline{C_{sat}} + O(\ln \varepsilon^2)$ where $\varepsilon = C_{sat} - \overline{C_{sat}}$, and we assume B to be an uniform constant, set to the global mean value. Then, we find an approximate expression for the global average of (13).

$$\delta \ln pCO_2^{atm} = B\delta \ln \overline{C_{sat}}. \tag{14}$$

Using (12, 14) to eliminate C_{sat} from (12), we find an expression for the sensitivity of $p\mathrm{CO}_2^{atm}$ to $\overline{C_{org}}$.

$$\frac{\delta pCO_2^{atm}}{\delta \overline{C_{org}}} = -\frac{V}{M\gamma} \tag{15}$$

$$\gamma \equiv 1 + \frac{V\,\overline{C_{sat}}}{BMpCO_2^{atm}}. \tag{16}$$

A dimensionless parameter, γ, emerges from the combination of the atmosphere-ocean carbon balance and the carbonate chemistry. It represents the relative size of the oceanic and the atmospheric carbon inventory, where atmospheric inventory is weighted with the Buffer factor. The second term on the RHS in Eq. (16) is on the order of 7 for the modern ocean. Therefore, to the leading order approximation, the sensitivity of atmospheric CO_2 to variation in $\overline{C_{org}}$ is independent of the size of the reservoirs.

$$\frac{\delta pCO_2^{atm}}{\delta \overline{C_{org}}} \sim -\frac{BpCO_2^{atm}}{\overline{C_{sat}}}. \tag{17}$$

These relationships (15, 17) are simple expressions for the sensitivity of atmospheric CO_2 to the soft tissue component, $\overline{C_{org}}$, which is directly coupled to the nutrient cycle through Eq. (7). Increasing the global inventory of $\overline{C_{org}}$ indicates an increase in the regenerated carbon and phosphate in the interior ocean, enhancing the relative importance of the biological path in the downwards transport of phosphate and carbon illustrated in Figure 3. The rate of variation in atmospheric CO_2 with respect to the change in $\overline{C_{org}}$ is set by the partial derivative, $\partial pCO_2^{atm}/\partial \overline{C_{org}}$, which essentially depends on globally averaged Buffer factor and the reference states of $\overline{C_{sat}}$ and $p\mathrm{CO}_2^{atm}$.

Now consider the partitioning of phosphate between the preformed pool and the regenerated pool. Variation in the soft tissue component, $\overline{C_{org}}$, is directly related to the changes in P^* through the integral constraint (9) and the definition of P^* (4).

$$\delta \overline{C_{org}} = R_{C:P}\delta \overline{P_{reg}} \tag{18}$$

$$= R_{C:P}P_0\delta \overline{P^*} \tag{19}$$

Combining Eqs. (15) and (19), we find

Table 1. Constants used in the theory

Symbol	Units	Value
$\overline{C_{sat}}$	μ mol kg^{-1}	1800
pCO_2^{atm}	ppmv	280
$R_{C:P}$	ND	106
$R_{N:P}$	ND	16
B	ND	10
γ	ND	6.10
V	m^3	$1.37 \cdot 10^{18}$
M	mol	$1.77 \cdot 10^{20}$

$$\frac{\delta pCO_2^{atm}}{\delta \overline{P^*}} = -\frac{VR_{C:P}P_0}{M\gamma} \sim 312\ ppmv \tag{20}$$

which is very similar to Eq. (15), but directly expressed in terms of the efficiency of the soft tissue pump, $\overline{P^*}$, which can only vary between 0 and 1 as long as the total phosphate inventory of the global ocean is conserved. It provides a constraint on the potential variation of atmospheric CO_2 with changes in the soft tissue pump. Atmospheric CO_2 can vary by approximately 300 ppmv between the minimum and the maximum efficiency of the soft tissue pump ($0 < \overline{P^*} < 1$), consistent with previous studies based on box models (Sarmiento and Toggweiler, 1984). (Constants used in this calculation are based on the modern ocean, shown in Table 1.) Sigman and Haug (2003) also showed that atmospheric pCO_2 is proportional to the globally averaged preformed nutrient in their box models through sensitivity studies. This simple theory is based on the combination of the mass balance for carbon and nutrients in the ocean-atmosphere system and the linearization of carbonate chemistry. Thus, the theory should hold as long as the applied perturbation does not cause significant changes in the Buffer factor.

d. Implications of P for potential changes in the soft tissue pump*

The theory predicts a simple response of atmospheric pCO_2 to perturbations in the inventory of regenerated phosphate, expressed in terms of $\overline{P^*}$. Climatological distributions of phosphate and oxygen indicate $\overline{P^*} = 0.36$ for the modern ocean (Conkright *et al.,* 2002). If $\overline{P^*}$ were to increase up to 0.7, the simple theory suggest that atmospheric CO_2 would be expected to decrease by 100 ppmv, which is similar to the difference in atmospheric pCO_2 between the Last Glacial Maximum (LGM) and the Holocene. What controls the possible range of variation in $\overline{P^*}$?

It is possible to consider the efficiency of the soft tissue pump, P^*, as a quasi-conservative tracer in the ocean based on the preformed phosphate.

$$P^* = 1 - \frac{P_{pre}}{P_0} \tag{21}$$

Global average of this equation, combined with Eq. (1, 9), becomes identical to Eq. (4). P^* carries similar information to the preformed phosphate in this formulation, but P^* has some notable properties.

- P^* cannot be greater than 1.
- P^* is conserved in the interior ocean.
- Water masses tend to exhibit distinct P^* concentrations.

In the modern ocean, the value of P^* in NADW is approximately 0.60, reflecting relatively low preformed phosphate concentration in NADW. The value of P^* is low ($\sim$0.15) in AABW, reflecting relatively high preformed phosphate in the Southern Ocean. Globally averaged P^* can be considered as the volume weighted mean of the P^* in the water masses in the global ocean. One could consider two possible methods to vary $\overline{P^*}$: (1) changing the phosphate concentration at the outcrop of isopycnals (P^* of the end members) and (2) changing the large-scale circulation in the oceans and volumetric ratio of various water masses. Both processes can lead to variations in $\overline{P^*}$.

Among the hypotheses for the glacial-interglacial variations in atmospheric CO_2, those based on the depletion of high latitude surface nutrients (Martin, 1990; Kumar *et al.,* 1995; Francois *et al.,* 1997) are essentially driven by the first mechanism with the changes in P^* of the end members. Alternatively, variations in the ocean circulation could have a large changes in the P^* distribution without changing the surface nutrient distribution (Toggweiler, 1999; Toggweiler *et al.,* 2003b), which is the second mechanism. Physical circulation determines the global distribution of P^* by mapping surface P^* distribution into the interior ocean. In summary the simple theory suggests that global changes in the soft tissue pump and its impact on atmospheric CO_2 can be quantified in terms of $\overline{P^*}$. Analysis based on P^* provides a simple and comprehensive diagnostic of the soft tissue pump.

In the following section we use an idealized, physical-biogeochemical model as a tool to examine the theory in the context of numerical simulation. The theoretical prediction (20) is tested against sensitivity experiments, and the simulated distribution of P^* provides useful insights into the mechanisms controlling the bounds on $\overline{P^*}$ and atmospheric CO_2.

3. Ocean-atmosphere carbon cycle model

In the simple theory, the sensitivity of atmospheric CO_2 to changes in the global inventory of P^* in Eq. (20) is calculated based on the integral constraints in the ocean-atmosphere system, combined with the carbon pump decomposition and the carbonate chemistry. The theory can be quantitatively tested in the context of numerical simulations. Furthermore it provides a theoretical framework to diagnose and interpret the simulated carbon pumps. Here we simulate ocean-atmosphere carbon cycle in an idealized bathymetry such that the model is computationally efficient and the results are easier to diagnose. The aims of the numerical experiments are to:

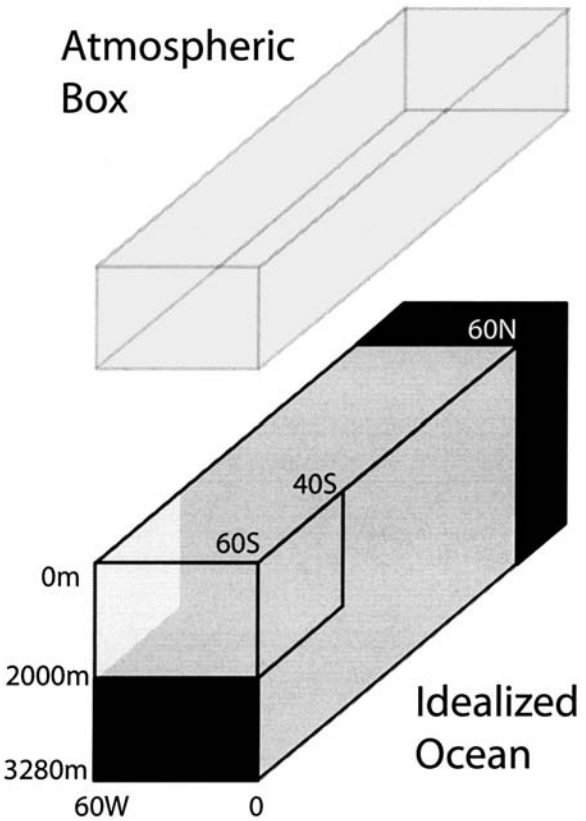

Figure 4. A schematic diagram of the idealized atmosphere-ocean carbon cycle model. The model is configured for a rectangular basin with an open channel in the southern hemisphere. Periodic boundary conditions are used for the latitudes between 40S and 60S from surface to 2000 m depth.

- Examine and illustrate simulated oxygen, phosphorus and carbon distribution using the concept of carbon pump components and P^*.
- Explicitly simulate the response of atmospheric CO_2 to the soft tissue pump, and test the theory such as Eq. (20) in a more complex setting.
- Explore the possible variations in P^* over a wide range of model parameters.

a. Model configuration and physical circulation

We use the MIT ocean general circulation and biogeochemistry model (Marshall *et al.,* 1997a,b; Follows *et al.,* 2002) configured in an interhemispheric, rectangular ocean basin with an open channel in the Southern hemisphere (Fig. 4). Polewards of 40S, a periodic boundary condition is applied to represent the circumpolar current, which extends to the southern boundary of the model domain (60S) and down to 2000 m. The model has flat bottom at 3280 m depth, horizontal resolution of 3° and 12 vertical levels of varying

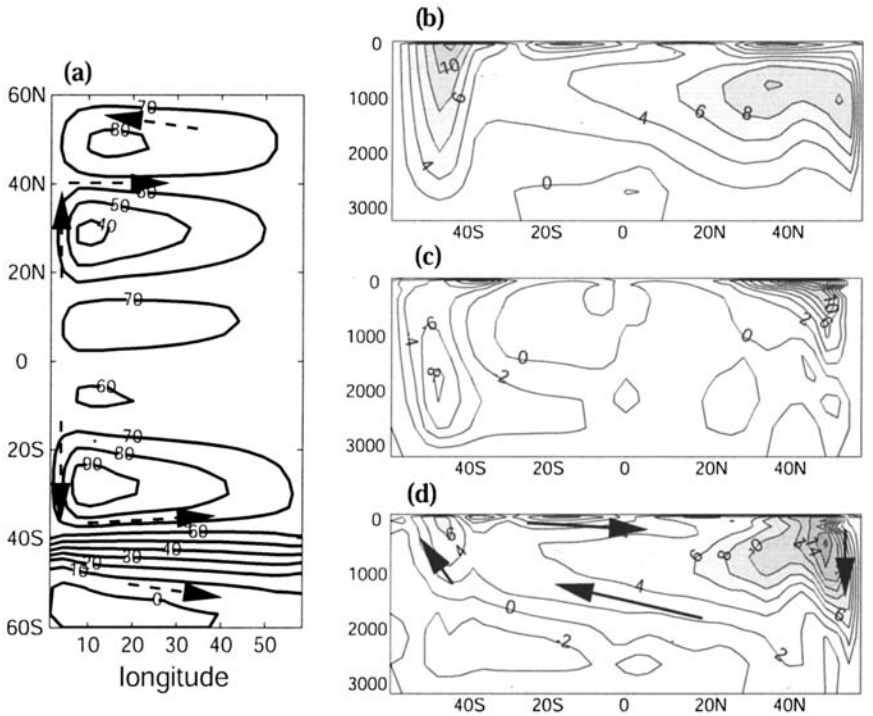

Figure 5. Steady state physical circulation. (a) Barotropic stream function is the depth integrated flow. Contour spacing is 10 Sv (b) Meridional overturning circulation is the zonally averaged overturning circulations. Contour spacing is 2 Sv. Top, middle and bottom panel represent Eulerian mean flow, eddy-induced flow and the "residual" (or "effective") flow. The residual circulation is the sum of the Eulerian mean and the eddy-induced circulation.

thickness from 50 m at the surface and 540 m at the bottom. Eddy-induced circulation is parameterized using an isopycnal thickness diffusion scheme (Gent and McWilliams, 1990) with isopycnal diffusivity of 1000 $m^2\ s^{-1}$. Small scale diapycnal mixing is parameterized with a uniform, vertical tracer diffusivity of $5 \cdot 10^{-5}\ m^2\ s^{-1}$. The model is forced with an idealized zonal wind stress which has sinusoidal profile broadly similar to the present climate. Salinity is set to a uniform constant (35 psu), and the model density is entirely determined by temperature. SST is restored to a prescribed sinusoidal profile broadly similar to modern ocean climatology, with a timescale of 30 days. There is no seasonal variation in the wind and thermal forcing. The model is initialized with a uniform temperature at rest, and spun up for 5000 years.

Figure 5(a) shows the barotropic stream function of the model at steady state. Wind-driven subtropical gyres are present in both hemispheres, and a weaker, subpolar gyre is also found in the northern hemisphere. In the subpolar southern hemisphere, the circumpolar current transports about 60 Sv. Figure 5(b) shows the Eulerian mean overturning

circulation including about 8 Sv of deep water formation in the northern basin, and the wind-driven overturning circulation in the southern hemisphere. Figure 5(c) shows the parameterized eddy-induced transport due to Gent and McWilliams (1990) parameterization. In the northern hemisphere, the eddy-driven overturning circulation and the Eulerian mean circulation have the same sign, enhancing the deep water ventilation in the northern hemisphere. In the southern hemisphere, the eddy-driven overturning circulation nearly cancels out the Eulerian mean circulation. Figure 5(d) shows the residual mean overturning circulation which is the net effect of the Eulerian mean and the eddy-induced transport, and drives the advective transport of tracers in the model. The meridional overturning circulation is reduced to approximately 6 Sv in the circumpolar current, and a weak bottom cell emerges. The idealized model captures a broad structure of the meridional overturning circulation of the Atlantic Ocean. The major difference between more complex, global circulation model and this model is the lack of the Pacific basin and relatively short residence time of the deep waters.

b. Biogeochemical model

The biogeochemical model includes oxygen, phosphate and DIC as passive tracers which include physical transports, biological uptake and remineralization and air-sea gas transfer.

$$\frac{\partial P}{\partial t} + \mathbf{u} \cdot \nabla P = \nabla \cdot \mathbf{K} \nabla P + \frac{\partial F_P}{\partial z} \tag{22}$$

$$\frac{\partial O_2}{\partial t} + \mathbf{u} \cdot \nabla O_2 = \nabla \cdot \mathbf{K} \nabla O_2 - R_{O2:P} \frac{\partial F_P}{\partial z} - \frac{K_W}{\Delta z_1} (O_2 - O_2^{sat}) \tag{23}$$

$$\frac{\partial C}{\partial t} + \mathbf{u} \cdot \nabla C = \nabla \cdot \mathbf{K} \nabla C + R_{C:P} \frac{\partial F_P}{\partial z} - \frac{K_W}{\Delta z_1} ([CO_2] - [CO_2]^{sat}). \tag{24}$$

The third term on the RHS of Eqs. (23, 24) is the air-sea exchange terms and is active in the surface layer only. K_W is the gas transfer velocity and Δz_1 is the thickness of the first vertical layer which is set to 50 m in this model. The surface water exchanges oxygen and CO_2 with the atmosphere using a constant K_W of $5 \cdot 10^{-5}$ m s^{-1}.

Biological uptake is parameterized as a linear damping of phosphate at the surface layer of the model where biological uptake depletes surface nutrients over a prescribed timescale τ_{bio}. F_P represents the downward flux of sinking organic material measured in units of phosphate.

$$F_P(z = z_1) = -\tau_{bio}^{-1} \Delta z_1 P \tag{25}$$

$$F_P(z < z_1) = F_P(z = z_1) \left(\frac{z}{z_1} \right)^{-0.85} \tag{26}$$

where z_1 is the depth of the bottom of the surface layer. The timescale for uptake, τ_{bio}, a global constant which controls the sinking organic flux, is varied from 1.5 months to 10 years in the sensitivity studies. The vertical profile of F_P is parameterized using the Martin function (Martin *et al.,* 1987) and we neglect burial at the sea floor. For simplicity, the production and transport of calcium carbonate is not parameterized in this model.

A well-mixed, atmospheric box is coupled to the ocean carbon cycle such that the partitioning of carbon between the atmosphere and the ocean is explicitly calculated in the model. The model conserves total amount of carbon in the atmosphere and the ocean. Atmospheric mixing ratio of CO_2 can adjust with the net air-sea CO_2 flux at each time step. Carbonate chemistry is solved assuming using a uniform alkalinity of 2300 μ eq kg^{-1} (including Boric acid, Silicic acid and Phosphoric acid (Millero, 1995)).

The model is initialized with uniform DIC, oxygen and phosphate concentrations, and atmospheric CO_2 of 278 ppmv. The control run is spun up for 5000 years with the fixed atmospheric pCO_2, and biological export timescale is set to 360 days. After 5000 years of integration, the model fields are very close to the steady state. Then, we further spin up the model allowing atmospheric pCO_2 to adjust with the net air-sea CO_2 exchange. After additional 1000 year of integration, modeled atmospheric pCO_2 is found at 270 ppmv.

c. Control run

Figure 6 shows the steady state distribution of (a) phosphate, (b) oxygen and (c) DIC for the control run. The large scale distribution of these tracers broadly resembles those observed in the modern North Atlantic. The newly formed deep water in the northern hemisphere is relatively depleted in phosphate and rich in oxygen. As the deep water travels southward, it accumulates regenerated phosphate and carbon. In the southern hemisphere, phosphate concentration is notably high relative to the observed phosphate concentration in the South Atlantic. The elevated phosphate concentration is partly due to the old "age" of the deep waters there, and the slow ventilation (upwelling) in the southern hemisphere. As Figure 5 shows, the compensation between the Eulerian mean flow and the eddy induced flow results in reduction of upwelling rate, allowing the regenerated phosphate and carbon to accumulate in the region. The subtropical thermocline is generally depleted in phosphate.

Figure 7 shows the steady state distribution of (a) preformed phosphate, (b) regenerated phosphate, (c) saturated component (C_{sat}) and (d) the degree of saturation (ΔC) for the control run. (We separate carbon pump components of the model using (3) through (8).) The model includes soft tissue pump only, and the regenerated phosphate and carbon are diagnosed using modeled oxygen distribution following (3) and (7). Modeled preformed phosphate in NADW is broadly similar to the observed pattern in the Atlantic section (Fig. 2a), however, there are significant differences in preformed phosphate between the idealized model and the observation in the Southern Ocean. Oxygen disequilibrium is relatively small in this model due to the lack of sea ice cover at high latitudes. Undersaturation of oxygen at high latitude southern hemisphere is on the order of -10 μM

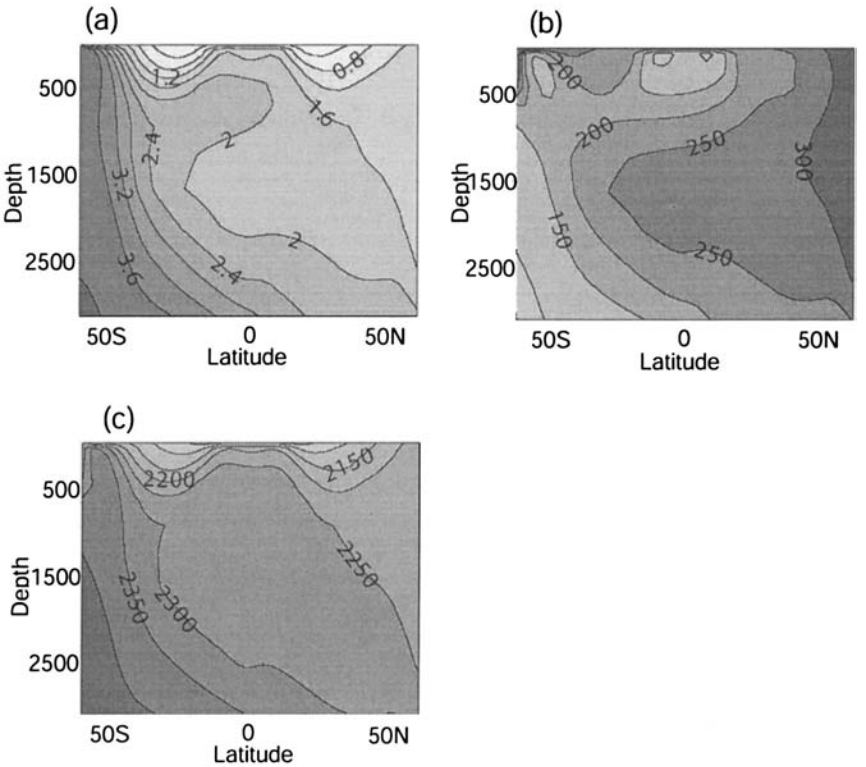

Figure 6. Modeled phosphate, oxygen and DIC in the control run. (a) Zonally averaged phosphate at steady state. Contour interval is 0.4 μM. (b) Zonally averaged oxygen at steady state. Contour interval is 50 μM. (c) Zonally averaged DIC distribution at steady state. Contour interval is 50 μM.

and associated error in C_{org} is on the order of 7 μM causing a slight overestimation of respiration.

In the deep ocean, the lowest P_{reg} is found in the newly formed deep waters in the northern hemisphere. As the deep water moves southwards, regenerated phosphate increases due to remineralization. P_{reg} has its maximum concentration in the southern hemisphere. Figure 7(c) shows the saturated carbon distribution with respect to atmospheric pCO_2 of 270 ppmv. It largely reflects the variation of solubility of CO_2 with the thermal structure of the ocean. Figure 7(d) shows the distribution of disequilibrium carbon component. The deep ocean is mostly undersaturated with respect to the atmospheric CO_2 in this particular model due to the effect of heat loss at the region of deep water formation.

The surface phosphate concentration is carried into the ocean interior as preformed phosphate, thus, the water masses show distinct P_{pre} concentration. In this model, the subtropical thermocline is depleted in P_{pre}, reflecting the high degree of surface nutrient utilization in this region. In the deep ocean, the newly formed deep waters in the northern

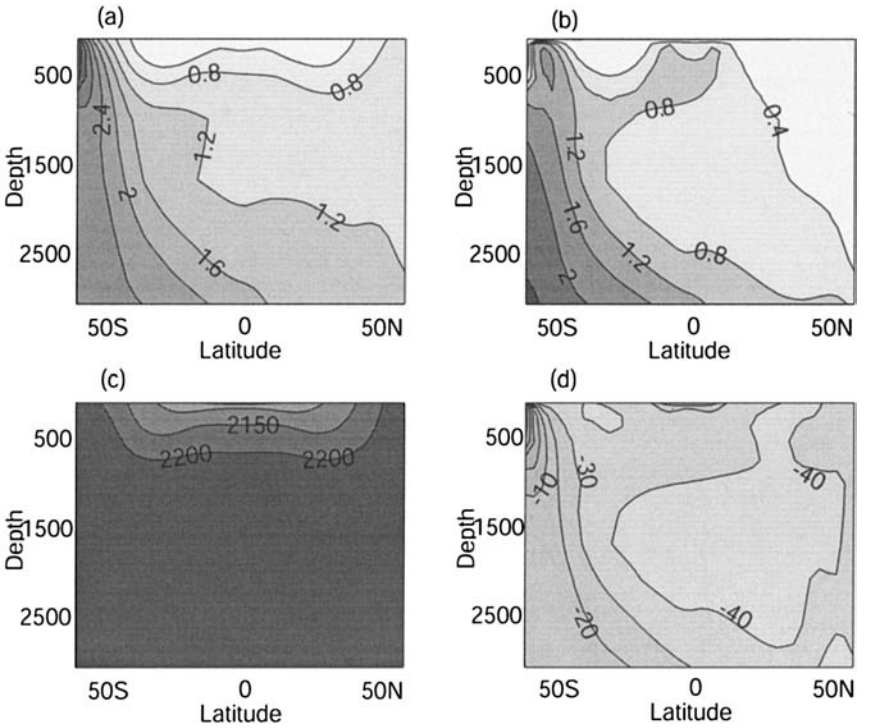

Figure 7. Zonally averaged carbon pump components at steady state in the control run. (a) Preformed phosphate, P_{pre}, in units of μM. Contour interval of 0.4 μM. (b) Regenerated phosphate, P_{reg}, with the same units and contour interval as (a). (c) Saturated carbon component, C_{sat}, in units of μM. Contour interval is 50 μM. (d) Disequilibrium component, ΔC, in units of μM. Contour interval is 10 μM.

hemisphere carry approximately 0.9 μ M of P_{pre}, somewhat similar to the observed P_{pre} in North Atlantic Deep Water (NADW) shown in Figure 2. In the southern hemisphere, the preformed phosphate concentration is very high, above 2.0 μM, reflecting high surface phosphate concentration.

Figure 5 reveals that a weak bottom overturning cell ventilates the deepest part of the ocean in the southern hemisphere. The formation of deep waters occurs at the southernmost grid near the western boundary of the model domain in this particular configuration. Polewards of the circumpolar current, the region of upwelling and the region of sinking are at similar latitudes. The upwelling deep waters are enriched in phosphate and carbon because of the integrated effect of remineralization. The biological uptake and export consume phosphate and carbon at the surface, however, the surface residence time of water is relatively short due to the convective mixing and the formation of deep waters. The upwelled water parcel leaves the surface layer before phosphate is completely utilized, and it maintains the large preformed nutrient concentration.

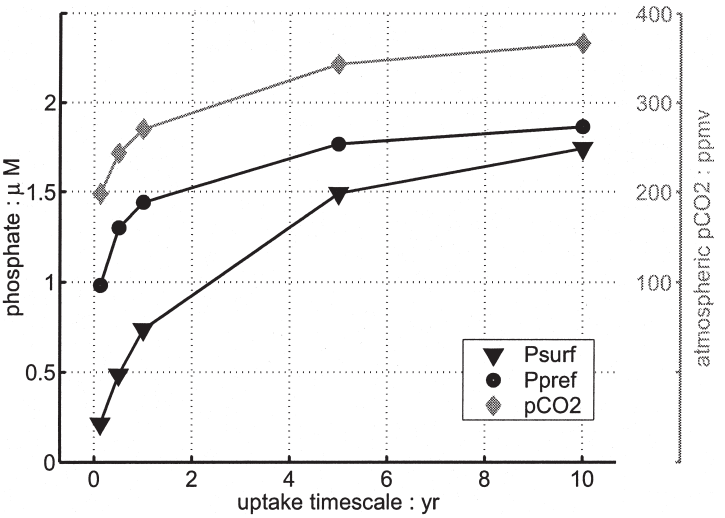

Figure 8. Simulated response of atmospheric CO_2, global mean P_{pre} and mean surface P to the variation of the biological uptake timescale.

d. Sensitivity run

We examine the sensitivity of atmospheric pCO_2 to a wide range of biological uptake parameter, τ_{bio}; from 1.5 months to 10 years. The total amount of carbon in the atmosphere and the ocean is conserved. Each experiment starts with the tracer distribution of the control run, and the model is spun up using different τ_{bio} for 1000 years. The response in atmospheric pCO_2 is evaluated.

Figure 8 shows the variation of atmospheric CO_2, globally averaged preformed phosphate and the surface average phosphate concentration. As the biological uptake timescale becomes shorter, rapid removal depletes surface phosphate and draws down atmospheric CO_2. The relationship between biological export rate and atmospheric pCO_2 is not linear.

Figure 9 shows the relationship between pCO_2^{atm} and $\overline{P^*}$ (and $\overline{P_{pre}}$), which is in a reasonable agreement with the theoretical prediction (20). The dashed line represents the sensitivity of atmospheric CO_2 predicted by the simple theory. The theoretical slope, $\partial pCO_2^{atm}/\partial\overline{P^*} = 312$ ppmv, and the intercept are chosen such that the theoretical sensitivity is referenced to the control run. The soft tissue pump is more efficient when preformed phosphate is drawn down by biological uptake. Atmospheric CO_2 varies from 200 ppmv to 360 ppmv corresponding to the variation of globally averaged P^* of 0.45. When the mean preformed phosphate is high (above 1.7 μM), the theory somewhat underestimates the sensitivity. As we illustrate later, the difference between the theoretical prediction and the results from sensitivity experiments is partly due to the response of ΔC, and the finite amplitude of the perturbation.

Figure 10 shows the relationship between global mean preformed phosphate and mean

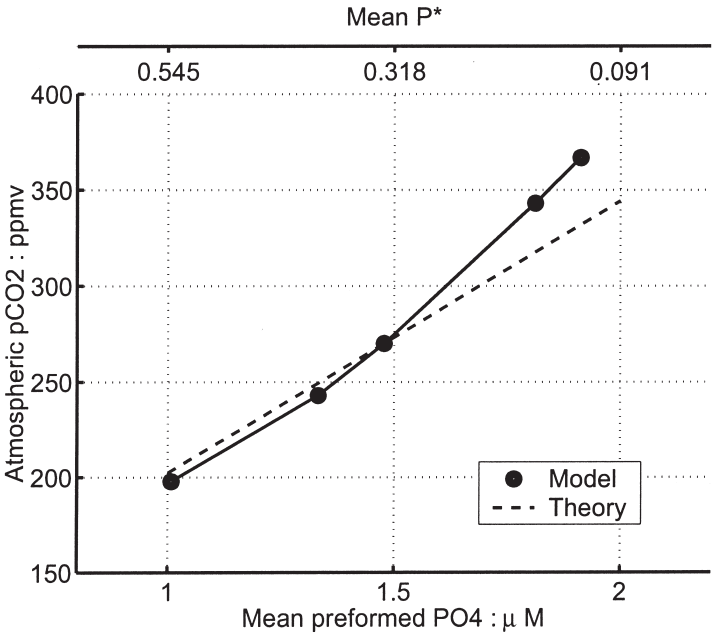

Figure 9. Simulated co-variation of atmospheric CO_2 to the global mean P_{pre}.

surface phosphate. We have used wide range of the biological uptake timescales from 1.5 months to 10 years. Even with the uptake timescale of 1.5 months, we still find $\overline{P^*} = 0.55$ suggesting that only 55% of dissolved phosphate is formed by respiration on the global average. In contrast, the corresponding mean surface phosphate is very low on the order of 0.22 μM. There is a strong decoupling of surface phosphate and preformed phosphate when biological uptake is very rapid. In a limit case where surface phosphate is completely depleted, we would expect $\overline{P^*}$ to be very close to 1 indicated by dash line in Figure 10. However, the export timescale of 1.5 months close to the reasonable biological limit for marine biological organisms. Physical transport plays a critical role in relating the surface phosphate distribution and the preformed phosphate in the interior ocean. Deep waters are formed in highly localized regions in the high latitude oceans. The properties of surface waters at these localized regions control the preformed properties of the global deep waters. Formation of deep waters may be associated with intense convective mixing which supports a locally elevated phosphate concentration in the region of deep convection. Figure 11 illustrates the convective supply of phosphate in the region of deep convection, which plays a critical role in setting the upper bound of P^* in the model. The preformed phosphate (and P^*) of deep waters is set at the outcrop of deep isopycnals which is largely decoupled from the rest of the surface oceans. Vertical supply of phosphate due to convective mixing is sufficient to support elevated preformed phosphate even when the biological export is very efficient ($\tau_{bio} \sim 1.5$ month). We suggest that the

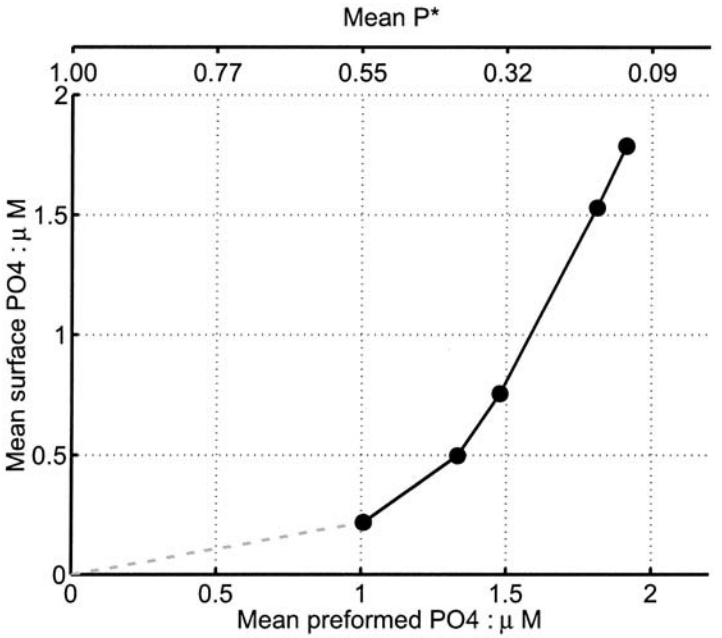

Figure 10. Relationship between the global mean P_{pre} and the mean surface P.

dynamics of the deep water formation limits the possible range of P^* and the efficiency of the soft tissue pump.

Table 2 shows detailed results of the sensitivity experiments, showing the variation of

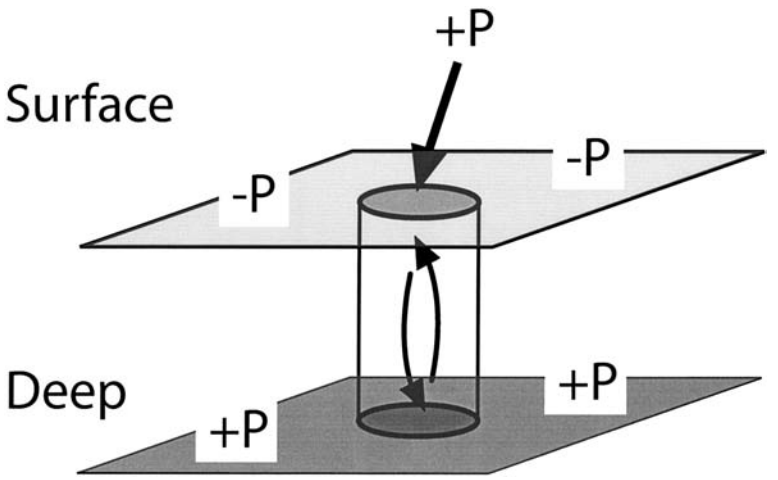

Figure 11. Preformed phosphate at a high latitude surface outcrop is elevated due to the vertical supply of phosphate through convective mixing.

Table 2. Results from sensitivity experiments. The leading order balance in (12) is between $\overline{C_{sat}}$ and $\overline{C_{org}}$. Since the oceanic reservoir of carbon is much larger than the atmosphere, the variations in the carbon pump components tend to cancel out within the ocean. The atmospheric reservoir does not play a leading role in the carbon mass balance, and pCO_2^{atm} simply covaries with the saturated component, $\overline{C_{sat}}$.

Model variable	Units	Exp1	Exp2	Control	Exp3	Exp4
τ_{bio}	days	45	180	360	1800	3600
pCO_2^{atm}	ppmv	198	243	270	343	367
$\overline{AOU}$	μM	196	141	117	60.3	43.4
$\overline{P_{surf}}$	μM	0.22	0.50	0.76	1.53	1.79
$\overline{P_{pre}}$	μM	0.98	1.30	1.44	1.77	1.87
$\overline{C_{reg}}$	μM	131	94.7	78.3	40.5	29.2
$\overline{\Delta C}$	μM	−5.65	−9.67	−13.6	−23.4	−25.6
$\overline{C_{sat}}$	μM	2057	2094	2112	2151	2161
$\bar{C}$	μM	2182	2179	2177	2168	2165

the global average of each carbon pump component and atmospheric $p\mathrm{CO}_2$ with corresponding values of τ_{bio}. We examine the carbon mass balance and diagnose the partitioning of carbon between the atmosphere and the ocean in order to better understand the carbon and nutrient balances in the model and evaluate the theory presented in Section 2c.

Figure 12 is a graphical summary of the data presented in Table 2, showing the variation of the global inventory of each carbon pump components. Each of the runs has different partitioning of carbon between the atmosphere and the ocean, and between different carbon pump components within the ocean. We examine the partitioning of carbon among four reservoirs; (1) atmosphere, $MpCO_2^{atm}$, (2) saturated component, $V\overline{C_{sat}}$, (3) regenerated component, $V\overline{C_{reg}}$ and (4) disequilibrium component, $V\overline{\Delta C}$. In Figure 12, the sum of variations in the four reservoirs (1) through (4) is always zero due to the global conservation of carbon. Partitioning of carbon changes significantly with the biological pump. The dominant balance is between the saturated component (2) and the regenerated component (4). As τ_{bio} increases (decreasing the biological uptake rate), the regenerated component decreases as a result of weaker biological pump. The decrease in $\overline{C_{reg}}$ is mainly balanced by the increase in $\overline{C_{sat}}$ consistent with the increase in atmospheric $p\mathrm{CO}_2$.

There is a relatively small change in the disequilibrium component in response to variations in the soft tissue pump. Simulated disequilibrium of CO_2 in polar outcrop is relatively large, on the order of -40 μM as shown in Figure 7(d). The distribution of ΔC in deep oceans reflects conditions at the polar outcrop. At high latitudes, surface waters are undersaturated in CO_2 because of the intense cooling and short residence time of surface waters in this region. Organic pump can influence air-sea CO_2 disequilibrium which has opposing sense from the effect of the air-sea heat flux at the polar oceans. When deep waters upwell and are entrained into surface layer at high latitudes, the surface water tends to be supersaturated because deep waters are enriched in phosphate and carbon through the integrated effect of remineralization, causing the outgassing of biologically sequestered

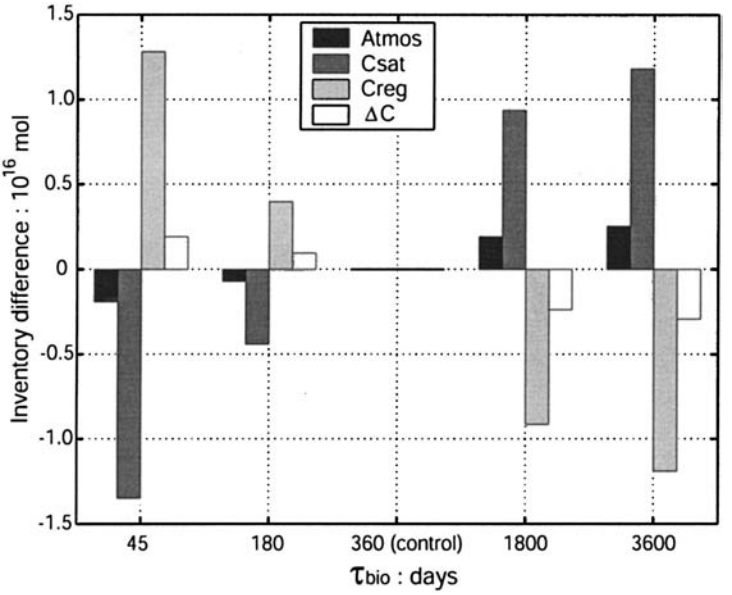

Figure 12. Carbon inventory difference relative to the control run. We consider the partition of carbon among four reservoir; (1) atmosphere, $MpCO_2^{atm}$, (2) saturated component, $V\overline{C_{sat}}$, (3) regenerated component, $V\overline{C_{reg}}$ and (4) disequilibrium component, $V\overline{\Delta C}$.

CO_2. Table 1 of Toggweiler *et al.* (2003b) illustrates this mechanisms in a simple box model. Changes in the rate of biological uptake and export can influence surface disequilibrium of CO_2 through this mechanism, however, the magnitude of variations in ΔC is small relative to the changes in C_{org} in these numerical experiments, and so it makes a minor correction to the simple theory. Figure 12 shows that $\delta\overline{\Delta C}$ and $\delta\overline{C_{org}}$ covary in the same sign. $\delta\overline{\Delta C} \sim 0.2\delta\overline{C_{org}}$. In the regions of deep water formation, particularly, to the south of the circumpolar current, surface residence time of water parcel is relatively short, and the newly formed deep waters maintain some degree of supersaturation as they are subducted again.

Can we quantify the effect of supersaturation on the efficiency of the soft tissue pump? Using (12) and (14), we can show that the sensitivity of atmospheric CO_2 to globally averaged ΔC is identical to (15):

$$\frac{\delta pCO_2^{atm}}{\delta\overline{\Delta C}} = -\frac{V}{M\gamma}. \tag{27}$$

The net response of atmospheric CO_2 to changes in both C_{org} and ΔC can be calculated by

$$\delta pCO_2^{atm} = \frac{\delta pCO_2^{atm}}{\delta\overline{C_{org}}}\,\delta\overline{C_{org}} + \frac{\delta pCO_2^{atm}}{\delta\overline{\Delta C}}\,\delta\overline{\Delta C} \tag{28}$$

$$= -\frac{V}{M\gamma}\{\delta\overline{C_{org}} + \delta\overline{\Delta C}\}$$

While the theory does not predict the response of ΔC, in the sensitivity experiments studied here, we find $\delta\overline{\Delta C} \sim 0.2\delta\overline{C_{org}}$. Thus, the air-sea disequilibrium enhances the effect of the biological pump by approximately 20%, a minor adjustment to the simple relationship (15).

4. Discussion

We have examined the relationship between atmospheric pCO_2 and the partitioning of phosphate between the preformed and regenerated pools using simple theory, observations and numerical experiments. Preformed phosphate is a clear signature of the major water masses in the oceans (Broecker *et al.,* 1985; 1998) and the associated P^*, which is defined in Eq. (21), can be used as an indicator of the efficiency of the organic pump. Analysis of observed phosphate and oxygen data suggests that P^* of newly formed NADW is on the order of 0.55 and that of AABW is on the order of 0.15. In the modern ocean, the value of the globally averaged P^* is approximately 0.36, indicating that 36% of phosphate returns to the interior ocean through biological export and remineralization. The soft tissue pump of the modern ocean is operating well below the theoretical maximum efficiency.

We develop a simple theory, combining the analysis of the carbon pumps with global conservation constraints, which predicts the relationships between the global mean P^* and atmospheric pCO_2. The theory predicts that atmospheric pCO_2 decreases by ~30 ppmv for 0.1 increase in globally averaged P^*. The predicted sensitivity of atmospheric CO_2 is clearly supported by a suite of experiments with a numerical ocean-atmosphere carbon cycle model, over a wide range of biological uptake rates. The numerical experiments also reveal that the disequilibrium of CO_2 at the sea surface responds to changes in the variations in the soft tissue pump, increasing the sensitivity of atmospheric pCO_2 approximately by 20%.

Since the modern diagnostics suggest that global deep ocean preformed phosphate is currently on the order of 1.4 μM (Broecker *et al.,* 1998; Conkright *et al.,* 2002) and the corresponding $\overline{P^*}$ is 0.36, it seems to suggest that there is sufficient potential for change in the soft tissue pump to cause a glacial scale draw down of pCO_2 (~100 ppmv). However, experiments with numerical models have not borne this out (Archer *et al.,* 2000). Such experiments have typically manipulated the surface PO_4 distribution through strong damping. It is implicitly assumed that very low surface nutrient concentrations must be equivalent to low preformed nutrient concentrations. However, the relationship between the surface nutrient distribution and global mean preformed nutrients (and P^*) is not clear, as we have emphasized earlier.

In our numerical experiments, the case with very rapid export of surface PO_4 (τ = 1.5 months) exhibited low surface nutrient concentrations (See, Fig. 10) almost everywhere but the global mean preformed PO_4, the property significant for the carbon pumps, is

still close to 1 μM. Deep waters are formed and ventilated at a few limited locations in the high latitude surface oceans, and the formation of deep waters is often associated with intense convective mixing which supports a locally elevated phosphate concentration. The dynamics of deep water formation limits the potential range of P^* at relatively low values (~0.55). Preformed phosphate and P^* of deep waters are set at the outcrops of deep isopycnals which are largely decoupled from the rest of the surface oceans. We suggest that box models, which show a much stronger response of pCO_2 to draw down of surface nutrients, typically have wider range in preformed phosphate and P^* due to the lack of representation of deep convection. Our theoretical predictions and numerical simulation indicate that the upper bound of $\overline{P^*}$ is ultimately set by the localized dynamics of deep water formation. This mechanism could ultimately control the efficiency of biological pumps even in a climate with higher rates of atmospheric dust deposition to the Southern Ocean.

We stress that the carbon pump analysis based on the concept of preformed and regenerated nutrients is the appropriate diagnostic framework for understanding and quantifying the relationships of biological activity and atmospheric CO_2. In order to better understand the existing body of numerical model experiments we suggest a reanalysis of the results and some effort to understand the relationships between mean surface ocean nutrient budgets and global mean preformed nutrients. With sufficient global data coverage it may be possible to quantify the current carbon pumps. The distributions of the preformed, regenerated and disequilibrium carbon pools provide a meaningful quantitative benchmark for comparison with modeled carbon pumps. We note that it is important that the regenerated components are evaluated with respect to the isopycnal outcrops using the concept of preformed properties of the waters (Broecker and Peng, 1982; Broecker *et al.,* 1985; 1998). Referencing changes to global surface mean properties (e.g. Gruber and Sarmiento, 2002), focusing on the mean vertical gradients (e.g. Volk and Hoffert, 1985), or relating the carbon pumps to the global surface ocean nutrient inventory (Archer *et al.,* 2000) leads to complications because the significant horizontal variations of properties are not accounted for.

Finally, our numerical model illustrates the compensation between C_{org} and C_{sat}: increasing the soft tissue carbon component is largely compensated by the reduction in atmospheric CO_2 and the resulting reduction in C_{sat}, such that global carbon inventory is conserved. In addition, the disequilibrium carbon pool, ΔC, responds to the changes of the biological pump, and the variation in the ΔC inventory has similar magnitude to that of the atmospheric CO_2 inventory, which makes some contribution to the amplification of the sensitivity of atmospheric pCO_2. The disequilibrium in regions of deep water formation reflects a complex interplay of the prior history of a water parcel, its residence time in the surface waters and the air-sea equilibration timescale for CO_2 (Toggweiler *et al.,* 2003a). We believe that it is important to better understand what sets ΔC in the deep water formation regions in order to understand our models and the diagnostics from the modern ocean carbon cycle.

Acknowledgments. We thank two anonymous reviewers who supplied helpful comments. T.I. is grateful for funding from the Office of Polar Program of NSF, and M.J.F. is grateful for funding from NSF (OCE-336839) and NOAA (NA16GP2988). This publication is partially funded by the Joint Institute for the Study of the Atmosphere and Ocean (JISAO) under NOAA Cooperative Agreement No. NA17RJ1232, Contribution #1120.

REFERENCES

Anderson, L. A. 1995. On the hydrogen and oxygen content of marine phytoplankton. Deep-Sea Res. I, *42,* 1675–1680.

Archer, D., G. Eshel, A. W. B. Winguth *et al.* 2000. Atmospheric co2 sensitivity to the biological pump in the ocean. Global Biogeochem. Cycles, *14,* 1219–1230.

Bolin, B. and E. Eriksson. 1959. Changes in the carbon dioxide content of the atmosphere and sea due to fossil fuel combustion, *in* The Atmosphere and the Sea in Motion, B. Bolin, ed., Rockefeller Inst. Press, 130–142.

Brewer, P. G. 1978. Direct observation of oceanic CO_2 increase. Geophys. Res. Lett., *5,* 997–1000.

Broecker, W. S. 1974. "NO" A conservative water-mass tracer. Earth Planet. Sci. Lett., *23,* 100–107.

Broecker, W. S., S. L. Peacock, S. Walker, R. Weiss, E. Fahrbach, M. Schroeder, U. Mikolajewicz, C. Heinze, R. Key, T.-H. Peng and S. Rubin. 1998. How much deep water is formed in the Southern Ocean? J. Geophys. Res., *103,* 15833–15843.

Broecker, W. S. and T. H. Peng. 1982. Tracers in the Sea, Eldigio Press, Palisades, NY, 690 pp.

Broecker, W. S., T. Takahashi and T. Takahashi. 1985. Sources and flow patterns of deep ocean waters as deduced from potential temperature, salinity, and initial phosphate concentration. J. Geophys. Res., *90,* 6925–6939.

Chen, G. T. and F. J. Millero. 1979. Gradual increase of oceanic CO_2. Nature, *277,* 205–206.

Conkright, M. E., R. A. Locarnini, H. E. Garcia, T. D. O'Brien, C. Stephens and J. I. Antonov. 2002. World Ocean Atlas 2001: Objective Analyses, Data Statistics, and Figures. CD-ROM Documentation. National Oceanographic Data Center, Silver Spring, MD.

Follows, M., T. Ito and J. Marotzke. 2002. The wind-driven, subtropical gyres and the solubility pump of CO_2. Global Biogeochem. Cycles, *16,* doi:10.1029/2001GB001786.

Francois, R., M. A. Altabet, E.-F. Yu, D. M. Sigman, M. P. Bacon, M. Frank, G. Bohrmann, G. Barielle and L. D. Labeyrie. 1997. Contribution of Southern Ocean surface-water stratification to low atmospheric CO_2 concentrations during last glacial period. Nature, *389,* 929–935.

Gent, P. R. and J. C. McWilliams. 1990. Isopycnal mixing in ocean circulation model. J. Phys. Oceanogr., *20,* 150–155.

Gruber, N. 1998. Anthropogenic CO_2 in the Atlantic Ocean. Global Biogeochem. Cycles, *12,* 165–191.

Gruber N. and J. L. Sarmiento. 2002. Large-scale biogeochemical interactions in elemental cycles, *in* The Sea, *12*, A. R. Robinson, J. J. McCarthy and B. J. Rothschild, eds., J. Wiley & Sons, NY, 337–399.

Gruber, N., J. L. Sarmiento and T. F. Stocker. 1996. An improved method for detecting anthropogenic CO_2 in the oceans. Global Biogeochem. Cycles, *10,* 809–837.

Ito, T., M. Follows and E. Boyle. 2004. Is AOU a good measure of respiration in the oceans? Geophys. Res. Lett., *31,* L17305, doi:10.1029/2004GL020900.

Knox, F. and M. B. McElroy. 1984. Changes in atmospheric CO_2—influence of the marine biota at high-latitude. J. Geophys. Res. Atmos., *89,* 4629–4637.

Kumar, N., R. F. Anderson, R. A. Mortlock, P. N. Froelich, P. W. Kubik, B. Dittrich-Hannen and M. Suter. 1995. Increases biological productivity and export production. Nature, *378,* 675–680.

Marshall, J., A. Adcroft, C. Hill, L. Perelman and C. Heisey. 1997a. A finite-volume, incompressible

navier stokes model for studies of the ocean on parallel computers. J. Geophys. Res., *102*(*C3*), 5753–5766.

Marshall, J., C. Hill, L. Perelman and A. Adcroft. 1997b. Hydrostatic, quasi-hydrostatic, and nonhydrostatic ocean modeling. J. Geophys. Res., *102(C3),* 5733–5752.

Martin, J. 1990. Glacial-interglacial CO_2 change: The iron hypothesis. Paleoceanogr., *5,* 1–13.

Martin, J., G. Knauer, D. Karl and W. Broenkow. 1987. Vertex: carbon cycling in the northeast pacific. Deep-Sea Res., *34,* 267–285.

Millero, F. 1995. Thermodynamics of the carbon dioxide system in the oceans. Geochim. Cosmochim. Acta, *59,* 661–667.

Petit, J. R., J. Jouzel, D. Raynaud, N. I. Barkov, J.-M. Barnola, I. Basile, M. Bender, J. Chappellaz, M. Davis, G. Delaygue, M. Delmotte, V. M. Kotlyakov, M. Legrand, V. Y. Lipenkov, C. Lorius, L. Pepin, C. Ritz, E. Saltzman and M. Stievenard. 1999. Climate and atmospheric history of the past 420,000 years from the vostok ice core, antarctica. Nature, *399,* 429–436.

Sabine, C., R. M. Key, F. J. Millero, A. Poisson, J. L. Sarmiento, D. R. W. Wallace and C. D. Winn. 1999. Anthropogenic CO_2 inventory of the Indian Ocean. Global Biogeochem. Cycles, *13,* 179–198.

Sarmiento, J. L. and J. C. Orr. 1991. Three-dimensional simulations of the impact of southern ocean nutrient depletion on atmospheric CO_2 and ocean chemistry. Limnol. Oceanogr., *36,* 1928–1950.

Sarmiento, J. L. and J. R. Toggweiler. 1984. A new model for the role of the oceans in determining atmospheric pCO_2. Nature, *308,* 621–624.

Schlosser, P., J. L. Bullister and R. Bayer. 1991. Studies of deep water formation and circulation in the Weddel Sea using natural and anthropogenic tracers. Mar. Chem., *35,* 97–122.

Siegenthaler, U. and T. Wenk. 1984. Rapid atmospheric CO_2 variations and ocean circulation. Nature, *308,* 624–626.

Sigman, D. M. and G. H. Haug. 2003. The biological pump in the past. Treatise on Geochemistry, *6,* 491–528.

Toggweiler, J. R. 1999. Variation of atmospheric CO_2 by ventilation of the ocean's deepest water. Paleoceanogr., *14,* 571–588.

Toggweiler, J., S. Carson and R. Murnane. 2003b. Representation of the carbon cycle in box models and GCMS: 2. Organic pump. Global Biogeochem. Cycles, *17,* doi:10.1029/2001GB001841.

Toggweiler, J., A. Gnanadesikan, S. Carson, R. Murnane and J. Sarmiento. 2003a. Representation of the carbon cycle in box models and GCMS: 1. Solubility pump. Global Biogeochem. Cycles, *17,* 1026. doi:10.1029/2001GB001401.

Volk, T. and Martin I. Hoffert. 1985. Ocean carbon pumps: Analysis of relative strengths and efficiencies in ocean-driven atmospheric CO_2 changes, *in* The Carbon Cycle and Atmospheric CO_2: Natural Variations Archean to Present, *32,* E. T. Sundquist and W. S. Broecker, eds., Geophysical Monograph, American Geophysical Union.

Weiss, R. R., H. G. Ostlund and H. Craig. 1979. Geochemical studies of the Weddel Sea. Deep-Sea Res., *26,* 1093–1120.

Received: *8 June, 2004;* revised: *10 February, 2005.*